RSC Advances

PAPER

View Article Online
View Journal | View Issue

Cite this: *RSC Adv.*, 2025, **15**, 41582

Application of a Sonogel-Carbon electrode modified with gold nanoparticles synthesized through a green technique and pine leaf extract for the simultaneous determination of neurotransmitters

Asma Blel,[ab] Juan José García-Guzmán,[c] Laura Cubillana-Aguilera,[c] José María Palacios-Santander *[c] and Chérif Dridi *[a]

This paper reports a Sonogel-Carbon electrode modified with pine leaf extract-derived gold sononanoparticles (AuSNPs) for the simultaneous detection of serotonin (5-HT) and dopamine (DA), key neurotransmitters in human health. To our knowledge, this is the first time AuSNPs have been greenly synthesized using pine leaf extract coupled with ultrasound technology in only a few minutes. The obtained AuSNPs (56 ± 14 nm) were characterized through several techniques: UV/vis spectroscopy, Fourier infrared spectroscopy, X-ray energy dispersive spectroscopy, and electron microscopy. The green AuSNPs were drop-cast onto the Sonogel-Carbon electrode (SNGCE) for the simultaneous determination of DA and 5-HT. The proposed sensor exhibited low limits of detection, good sensitivity (421.80 pM for DA and 192.55 pM for 5-HT), and reproducibility (RSD 4%). Proof of concept was demonstrated by their successful detection in human blood serum, obtaining recovery rates close to 100% for both analytes in all cases, demonstrating that this sensor has great potential for applications in neurodegenerative diseases and early-stage cancer diagnosis.

Received 1st July 2025
Accepted 13th October 2025

DOI: 10.1039/d5ra04658k

rsc.li/rsc-advances

1 Introduction

The development of rapid and sensitive devices for the simultaneous detection of neurotransmitters has critical implications for the clinical field and for the management of several diseases.[1] Alzheimer's and Parkinson's diseases, autism, schizophrenia, depression, cancer and anxiety[2] are great healthcare challenges for which early diagnosis and personalized therapies are of great concern. Recent studies have highlighted the therapeutic potential of compounds like chinonin in modulating neurotransmitter systems, offering new avenues for treating neurological disorders.[3] Dopamine (DA) has a significant impact on the brain system,[4,5] and it also affects the functioning of the cardiovascular, renal, hormonal, and central neurological systems.[6,7] Serotonin (5-hydroxytryptamine, 5-HT) is also found in several locations in the human brain and is essential for controlling one's mood, sleep, and hunger, among other functions.[8]

Neurotransmitters are crucial for the functioning of the nervous system. Notably, dopamine, categorized under catecholamines, and serotonin, classified as indolamines, are currently a focal point in the medical community. Changes in the concentration levels of these neurotransmitters have been linked to diverse physiological activities such as movement, learning, attention, cognition, libido, memory, depression,[9] bipolar disorder, and binge eating,[10] among others.

DA and 5-HT are relevant in the development of tumors; both are involved in cancer cell proliferation, progression, and metastatic processes, according to multiple studies. Increased secretion of serotonin and dopamine has been related to several cancers, including colorectal, prostate, small-cell lung cancer (SCLC), cholangiocarcinoma, hepatocellular carcinoma (HCC)[11] and breast cancer.[12] The normal human 5-HT levels in body fluids are between 0.5 nM and 15 nM, from 295 nM to 687 nM in urine, in the range of 270–1490 nM in serum samples,[2] about 500–1200 nM in whole blood and below 0.0591 nM in the cerebrospinal fluid.[13] DA, in combination with anticancer drugs, significantly inhibits tumor growth and increases the life span when compared with treatment with dopamine or anticancer drugs alone.[14] Therefore, the regulation of dopamine

[a]*NANOMISENE Laboratory, LR16CRMN01, Centre for Research on Microelectronics and Nanotechnology (CRMN) of Technopole of Sousse, B. P334, 4054 Sahloul, Sousse, Tunisia. E-mail: Cherif.Dridi@crmn.rnrt.tn*

[b]*University of Sousse, High School of Sciences and Technology of Hammam, Sousse, Tunisia*

[c]*Institute of Research on Electron Microscopy and Materials (IMEYMAT), Department of Analytical Chemistry, Faculty of Sciences, Campus de Excelencia Internacional del Mar (CEIMAR), University of Cadiz, Campus Universitario de Puerto Real, Polígono del Río San Pedro S/N, 11510 Puerto Real, Cadiz, Spain. E-mail: josem.palacios@uca.es*

and serotonin levels in human blood is crucial for maintaining physical, as well as mental and emotional well-being.

In this context, there have been several reports on the use of various methods, such as high-performance liquid chromatography (HPLC)[15] with electrochemical (EC) detection and mass spectrometry (MS),[16] enzyme-linked immunosorbent assay (ELISA),[17] thin layer chromatography (TLC),[18] coulometry,[19] fluorimetry, and chemiluminescence[20] to simultaneously quantify the levels of DA and 5-HT in real samples, such as biological fluids, nervous tissue, and pharmaceutical formulations.[21] Nevertheless, these techniques have some drawbacks, including high implementation costs, difficult sample pretreatment, long analysis times, and significant organic solvent consumption, which render them unsuitable for routine analysis. Therefore, electrochemical sensors[22] have been proposed as possibly the most advantageous methods for the simultaneous determination of both neurotransmitters, reducing the time of analysis by removing the need for sequential testing and resources. In fact, they have gained much attention owing to their rapidity, high sensitivity and selectivity, low cost, inherent simplicity, and ease of manipulation.[3,23]

In this regard, many of the electrochemical sensors used to determine DA and 5-HT are based on different polymers, nanomaterials, and/or biomolecules as modifiers, with several studies reporting the use of advanced functional nanomaterials to improve sensitivity and selectivity.[24,25] The employment of a green alternative to synthesize both the transducer and the modifiers would be an invaluable development. In fact, green-synthesized nanoparticles have become significant modifiers for electrochemical devices.[26] Due to their unique physicochemical properties, including superior conductivity, high surface-to-volume ratio, good biological compatibility, and strong electrocatalytic activity,[27] gold nanoparticles (AuNPs) are the focus of many studies, showing enormous potential for improving the performance of electrochemical (bio)sensors.[28–31]

Many studies have established the environmentally friendly and economically viable production of nanoparticles by employing various biomass resources, such as yeast, algae, fungi, and plants, to synthesize this kind of nanomaterial.[32] This is in contrast to the typical chemical method for synthesizing AuNPs[33] using potentially hazardous and toxic chemicals, which hinders their applicability in fields like biology and medicine. In this context, the use of plant extracts such as pine, olives, mint, *etc.*,[34,35] for the synthesis of metal nanoparticles has gained significant attention due to the straightforward approach, cost-effectiveness, and environmental benefits. Plant extracts are rich in enzymes, proteins, amino acids, polysaccharides, and phenolic compounds, which act as reducing agents in nanoparticle formation. Besides, these bioactive compounds create a stabilizing layer, preventing agglomeration and ensuring long-term stability.

While numerous studies have already exploited diverse plant extracts as reducing and stabilizing agents for AuNP synthesis, our work distinguishes itself by combining pine leaf extract, rich in tannins and phenolic compounds, with a high-energy ultrasound-assisted sonocatalysis process. This dual approach enhances the reduction kinetics and nanoparticle stability, and also provides a faster, greener, and more reproducible pathway compared to the conventional green synthesis routes.

This plant-mediated synthesis method is highly efficient due to the diverse metabolites involved, with high yields and exceptional stability across various plant species. For instance, recent research suggests that tannic acid-rich plants have significant potential for stable nanoparticle production. Additionally, the resulting nanomaterial gains value if the synthesis process is carried out utilizing a rapid, efficient, and environmentally friendly instrumental technique like high-energy ultrasound.[36] Siwar *et al.*[37] reported the green synthesis of gold nanoparticles using geranium leaf extract, while Geetha *et al.*[38] used *C. guianensis* for the same purpose. In both cases, they focused on the morphological and structural properties of the AuNPs and their potential as affordable, eco-friendly materials for biosensor development.

Over the past four years, several papers have focused on the simultaneous detection of both neurotransmitters, DA and 5-HT. J. Suriyaprakash *et al.* successfully developed a 2D-Bi_2S_3 biosensor *via* a two-step synthetic approach. The sensor's active surface demonstrated excellent electrochemical activity towards DA and 5-HT detection, exhibiting LODs of 54 nM and 68 nM, respectively.[39] Alternatively, S.H. KO *et al.*[40] reported the integration of PEDOT:PSS/Nafion(rGO-PP/NF) hybrid material for DA and 5-HT sensing applications. Good sensitivities of 99.3 and 86 $\mu A/\mu Mcm^2$, as well as low detection limits of 0.17 and 0.16 μM, for DA and 5-HT, respectively, were reported. Moreover, composites using Cu and CuO-based materials were employed for the development of highly sensitive biosensors for the simultaneous determination of 5-HT and DA[41–43] with very good performance. However, additional steps like heat treatment, capping agents, and calcination were involved in nanocomposite fabrication. Other reports have highlighted complex structures for the efficient simultaneous detection of 5-HT and DA.[10,36,44,45] Although the mentioned works demonstrate excellent electrochemical detection performance characterized by high sensitivity, good selectivity, and low limits of detection, the complexity of the biosensor fabrication processes and the costs associated with nanocomposite preparation remain significant challenges.

While prior studies have demonstrated excellent analytical performance with high sensitivity, good selectivity, and low detection limits, many involved complex fabrication processes, costly nanocomposites, or additional steps such as heat treatment and capping agents. In contrast, our proposed green, ultrasound-assisted AuSNP-based sensor provides a simple, eco-friendly, and highly efficient alternative. This comparison underscores the novelty and practical advantages of our approach.

Despite these remarkable advances, most reported platforms still exhibit certain limitations when directly compared. For example, Bi_2S_3- and CuO-based nanostructures provide nanomolar detection limits but involve multi-step synthesis, calcination, or capping agents that hinder scalability.[35–39] In contrast, PEDOT:PSS/Nafion(rGO-PP/NF) hybrids demonstrate good sensitivity and fast response, yet their electrochemical stability in complex biological matrices remains limited.[36]

While noble metal polymer composites achieve efficient DA and 5-HT separation, their fabrication procedures are often costly and time-consuming, thus restricting their translation into routine clinical analysis.[40,41] This comparative overview highlights the trade-off between sensitivity, selectivity, and fabrication simplicity, and justifies the exploration of greener, more straightforward, and eco-friendly strategies.

Very recent developments in next-generation electrochemical sensors have been reported, demonstrating highly sensitive and selective platforms for neurotransmitter detection.[46] This study particularly emphasizes the importance of integrating eco-friendly nanomaterials and advanced fabrication approaches, which is directly in line with our work. By adopting a green, ultrasound-assisted synthesis of AuSNPs, our strategy addresses ecological and economic considerations while maintaining high sensitivity and selectivity for DA and 5-HT detection.

In this work, to the extent of our knowledge, for the first time, gold sononanoparticles (AuSNPs) were synthesized using fresh pine leaf extract, with biomolecules serving both as reducing and capping agents, and a high-energy ultrasound-assisted sonocatalysis process. The green, simple, and fast fabrication procedure of the AuSNPs addresses ecological and economic concerns. The AuSNPs/SNGCE, also based on a green synthesized material (Sonogel-Carbon), demonstrated high sensitivity and selectivity for simultaneous DA and 5-HT detection. Additionally, the proposed nanosensor was successfully evaluated in real applications for the simultaneous detection of these neurotransmitters in blood serum, demonstrating an excellent recovery rate, which underscores its potential precision and reliability in practical sample analysis.

2 Experimental procedure

2.1 Reagents and materials

All reagents were used without further purification. Serotonin (5-HT), dopamine (DA), sodium dodecyl sulfate (SDS > 99%), and bentonite were purchased from Sigma-Aldrich (Germany). Dipotassium phosphate (K_2HPO_4) was purchased from Panreac (Spain), and monopotassium phosphate (KH_2PO_4 > 99.5%) was obtained from Merck, (Germany) and used to prepare the phosphate buffer solution. Methyltrimethoxysilane (MTMOS, 98%) was also purchased from Merck (Germany). Potassium gold(III) chloride ($KAuCl_4$, 99.99%) was obtained from Sigma-Aldrich (Germany), and pine leaves were directly collected from the same pine specimen, when necessary, from the gardens of the Faculty of Science at the University of Cadiz (Spain), and used to prepare the gold nanoparticles. Nanopure (18 MΩ cm) water from the Wasser Lab Ultramatic Plus (Type I) system (Barbatáin, Navarra, Spain) was utilized to prepare the aqueous solution. For the real sample tests, human blood samples were collected from different healthy volunteers at the facilities of the University Hospital of Puerto Real (Cádiz, Spain). The collection procedure was carried out at 25 ± 2 °C, under strict adherence to ethical guidelines and protocols, ensuring the consent of all the donors prior to the procedure.

2.2 Instrumentation

Electrochemical measurements were performed using an Autolab 302N potentiostat/galvanostat (Ecochemie, The Netherlands) connected to a PC running the software GPES. The SNGCE was the working electrode, with an inner diameter of 1.15 mm; a platinum rod served as the counter electrode, and a Ag/AgCl (KCl 3M) electrode was used as the reference electrode. AuSNPs and SNGC materials were synthesized with a high-energy ultrasound generator, specifically the SONICATOR 3000 developed by MISONIX Inc. (Farmingdale, NY, USA). The pine leaf extract was produced using a high-energy SONOPLUS HD2200 ultrasonic homogenizer from BANDELIN (Berlin, Germany). Verification of AuSNPs synthesis was conducted using a UV-visible spectrophotometer (JASCO, Maryland, USA) operating within the 400–900 nm range, utilizing a 2 mL cuvette and conducting the analysis at room temperature. To identify the functional groups in the pine leaf extract, responsible for NPs synthesis and stabilization, a Fourier transform infrared (FTIR) spectrophotometer (Shimadzu Corporation, Kyoto, Japan) was employed, and spectra were obtained in the range of 4000–400 cm^{-1}. The size, composition, and morphology of the AuSNPs were determined using scanning electron microscopy (SEM-FEI Nova NANOSEM 450, USA) in scanning/transmission mode at an acceleration voltage of 20 kV, coupled to an X-ray energy dispersive spectroscopy (EDS) analyzer. For the STEM images, an optimized quantity of AuSNPs was deposited onto the surface of a Cu/C grid (ANANE, Spain) and allowed to dry at room temperature in the absence of light. Moreover, SEM images of the surface of two SNGCEs modified with the AuSNPs were also obtained, following a similar drop-casting procedure. One of the electrodes selected was not used in any electrochemical measurement, whereas the other electrode had undergone at least 60 cycles of electrochemical determination for DA and 5-HT. The objective of this characterization was to investigate the presence of AuSNPs on the electrode surface, even after many uses of the modified sensing device.

2.3 Pine leaf extract preparation and AuSNPs synthesis

Here, 2 g of washed pine leaves were chopped and mixed with 10 mL of water, then sonicated at 25% amplitude for 5 minutes. After filtration, 20 mg of bentonite was added and stirred to remove proteins. The solution was filtered and refrigerated for 24 hours. Next, 1.25 mL of 1.5 mM $KAuCl_4$ was added to a glass vessel, followed by 70 μL of pine leaf extract after 30 seconds. After 3.5 minutes of sonication, the solution turned wine-red, indicating AuSNP formation. The corresponding preparation and synthesis procedure are shown in Scheme 1.

2.4 Fabrication of the AuSNPs/SNGC sensor

SNGC electrodes were prepared as discussed in our previous report.[47] Briefly, in a glass vessel, high-energy ultrasound was used to treat a mixture of 500 mL of MTMOS and 100 mL of 0.2 M HCl for 10 s. The resultant sonosol was then mixed thoroughly with 500 mg of graphite powder. The finished

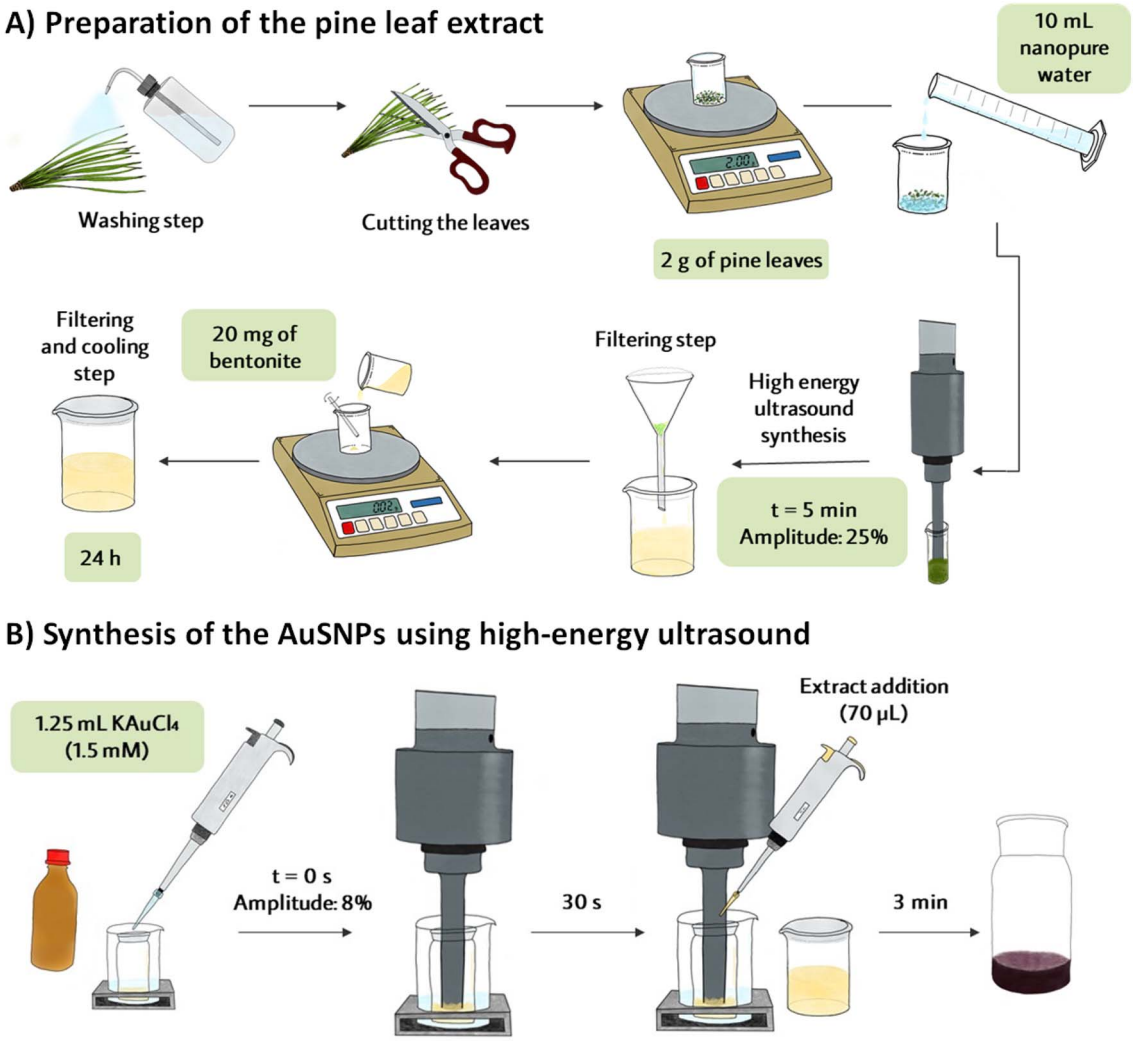

Scheme 1 (A) Pine leaf extract preparation. (B) Synthesis of the AuSNPs using high-energy ultrasound.

product had enough consistency after three minutes to fit into the glass capillary tubes with a 5 mm length. After 24 hours, the Sonogel-Carbon composite electrode surface was polished to remove any remaining composite material and create a smooth, mirror-like appearance using no. 1200 emery paper (Struers, Germany) and white satin paper. By placing a copper wire within the capillary tubes in close proximity to the electrodes, electrical contact was made. The gold sononanoparticles-based electrode was prepared by drop-casting 4 µL of AuSNPs solution onto the pre-cleaned SNGCE using a micropipette. The electrodes were then allowed to dry at room temperature in a dark environment.

2.5 Electrochemical measurements setup

All electrochemical measurements were carried out under ambient conditions. The experiments were conducted in the presence of 10^{-3} M of DA and 10^{-4} M of 5-HT in PBS (0.1 M) within the pH range of 3.0–9.0 and 4.0–8.0, for DA and 5-HT, respectively. Differential pulse voltammetry (DPV) was used as the electroanalytical technique in of potential range from 0 to 0.5 V, at intervals of 0.2 s (DA), 0.4 s (5-HT), and 0.2 s (DA + 5-HT) for repeatability and reproducibility assessments. The pulse amplitude of DA, 5-HT, and DA + 5-HT was 100 mV. The step potentials of DA, 5-HT, and DA + 5-HT were 4, 16, and 8 mV, respectively. Cyclic voltammetry (CV) was also performed at different scan rates ranging from 10 to 180 mV s^{-1}. To further investigate the electrochemical behavior of the proposed sensor, the selectivity of the device was evaluated by adding different concentrations of boric acid (BA), tryptophan (L-Trp), tyrosine (L-Tyr), ascorbic acid (AA), and calcium (Ca^{2+}) ions. For validation purposes, the sensor was tested using real serum samples under ambient conditions, and different parameters were extracted through the DPV technique.

3 Results and discussion

3.1 AuSNPs characterization

3.1.1 UV-visible spectroscopy. The addition of pine leaf extracts to the $KAuCl_4$ solution resulted in shifting the reaction mixture color from yellow to wine-red, as indicated in Fig. S1 of

the SI file. Because of the active antioxidant biomolecules in the aqueous pine leaf extracts, the Au^{3+} ions were reduced to Au atoms, which formed nanoclusters until the AuSNPs were obtained. Due to ultrasound irradiation, the conversion of the metal ions is quick and results in a stable AuSNPs colloid.

The characteristic surface plasmon resonance (SPR) band at the wavelength of 538 nm is typical of the AuSNPs, supporting the formation of AuSNPs (Fig. 1a). These studies are consistent with the results reported in the literature, where this characteristic SPR band generally appears between 520 and 550 nm.[27,48,49] The size distribution, as well as the average size ± standard deviation, was obtained from the STEM measurements. According to these results, the proposed pine leaf extract and high-energy ultrasound synthesis procedure generated AuSNPs between 30-80 nm, specifically 56 ± 14 nm, with approximately 80% of the nanoparticles having an average size of 54 nm as depicted in the histogram appearing in Fig. 1b.

We characterized the surface charge of the synthesized AuSNPs by zeta potential analysis and obtained a value of +79.8 mV, which indicated a highly stable colloidal suspension. It is well established that nanoparticles with zeta potential values above ±30 mV are considered electrostatically stable due to sufficient repulsive forces that prevent aggregation. Thus, the relatively high positive zeta potential of our AuNPs confirms their suitable long-term colloidal stability.[50]

3.1.2 FTIR characterization. Fig. 2 displays the typical FTIR spectra of both the pine leaf extract and the synthesized AuSNPs, revealing the involvement of key functional groups in the reduction and stabilization process. The broad band at 3311 cm^{-1} is due to –OH stretching vibrations of hydroxyl groups, most likely derived from polyphenols, which are known to donate electrons for the reduction of Au^{3+} ions and to form hydrogen bonds that contribute to nanoparticle stabilization.[51] The signals at 2334–2329 cm^{-1} are attributed to C≡C groups (alkyne), indicating additional stabilization effects through interaction with the nanoparticle surface.[52] The bands observed at 1635–1632 cm^{-1} correspond to C=O stretching vibrations of

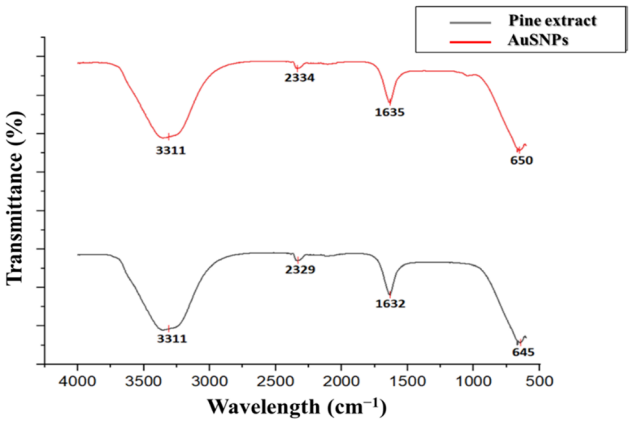

Fig. 2 FTIR spectra of the AuSNPs colloid and the pine leaf extract solution.

carbonyl groups, which can participate in the reduction of metal ions and establish coordination interactions with the AuSNPs surface. The bands at 650–645 cm^{-1} are associated with C–H and C–C vibrations, reflecting the presence of aromatic compounds and terpenoids that enhance colloidal stability.[53] The FTIR spectra of both the pine extract and AuSNPs exhibit similar characteristic bands, indicating the presence of key functional groups such as hydroxyl, alkyne, and carbonyl groups.[10,54] These groups are likely derived from polyphenols and flavonoids present in the pine leaf extract, which are responsible for the reduction and stabilization of AuSNPs during the biosynthesis process.

3.1.3 STEM and SEM analysis. On the one hand, AuSNPs were morphologically and compositionally characterized by STEM coupled with EDS (Fig. 3). From the STEM micrographs (Fig. 3a), it is possible to infer different sizes and shapes for the AuSNPs, showing the typical heterogeneous morphology of this kind of nanomaterial when synthesized using plant extracts:[55] spherical, triangular, polyhedral and nanorod-like shapes,

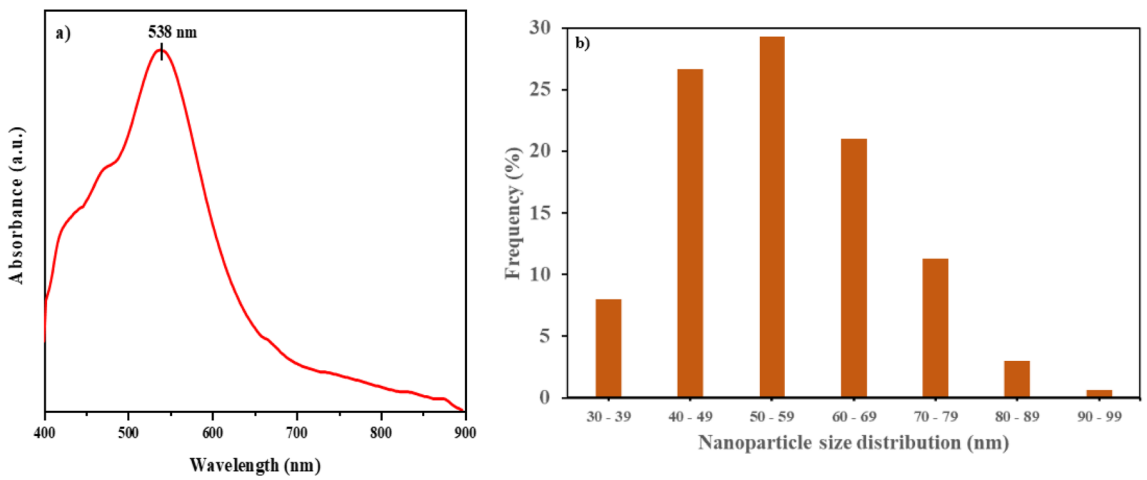

Fig. 1 (a) UV-visible spectrum of the AuSNPs colloid obtained after the synthesis with pine leaf extract and high-energy ultrasound technology. (b) Histogram built from STEM measurements.

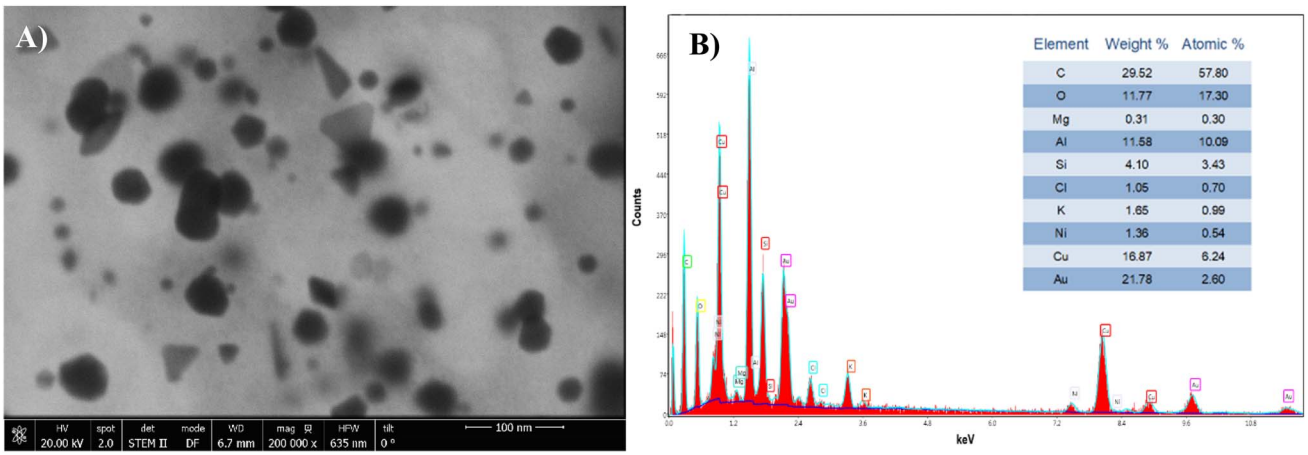

Fig. 3 (A) STEM micrograph of AuSNPs obtained after the synthesis with pine leaf extract and high-energy ultrasound technology (20 kV; × 200 000 magnification; and dark field mode). (B) EDS spectrum of the AuSNPs sample and a table showing the results of the corresponding semi-quantitative analysis.

among others. Furthermore, as mentioned previously, an average size of 56 ± 14 nm can be directly calculated from the different micrographs obtained ($n = 300$, where n is the number of AuNPs counted). Regarding composition (Fig. 3b), the EDS spectrum indicates clearly the presence of Au element in the sample, and the existence of other elements can be also justified: C and O, originate from the organic matter of the pine leaf extract; Cu and Ni, from the grid (apart from C); Si and Al, from the sample holder and the STEM detector; K and Cl, from the gold precursor.

SEM micrographs were also taken from the surface of two SNGC electrodes modified with AuSNPs at different magnifications: one electrode was not used, and the other electrode was used many times for electroanalytical measurements (see Fig. S2a–d in SI material). The micrographs were obtained using the back-scattered electron detector, which highlights elements of high atomic number (as Au). The micrographs show numerous white specks (corresponding to high Z values) that stand out against the black background (the Sonogel-Carbon material) and correspond to the gold nanoparticles deposited on the electrode surface. These micrographs also suggest the presence of AuSNPs throughout the entire electrode surface, although the number of specks did not seem to be significantly diminished due to leaching during electrochemical measurements. The observable wide gaps and fissures in the SNGC material are usually caused by erosion during the polishing step after its fabrication and during the measuring process. Fig. S3e shows, as an example, the EDS spectrum of the unused AuSNPs/SNGCE surface. This spectrum confirms the presence of the AuSNPs through the Au signals; other more intense signals corresponding to Si, C, and O, from the network of the SNGC material, were observed. Na, Ca, Cl, and Mg might have their origin in the extract or AuSNPs precursors. Ti peaks correspond to the SEM sample holder. In the EDS spectrum of the used electrode (not shown), other peaks related to P, K, and Na appeared, which may come from the buffer solution employed for the measurements.

3.2 Electrochemical behavior of AuSNPs/SNGCE

The electrochemical performance of the prepared SNGCE/AuSNPs electrode was assessed by cyclic voltammetry (CV) in 0.5 M KNO_3 containing 5 mM $K_4[Fe(CN)_6]$ as the redox probe. As shown in Fig. 4a, the CV curves of SNGCE and SNGCE/AuSNPs clearly illustrate the effect of AuNP modification. Compared to the bare SNGCE, the SNGCE/AuSNPs electrode exhibited a 44% increase in the anodic peak current and a 38% increase in the cathodic peak current, demonstrating the enhanced electrocatalytic activity and accelerated electron transfer provided by AuSNPs.

Electrochemical impedance spectroscopy (EIS) further confirmed this improvement. The impedance spectra were fitted using a Randles equivalent circuit model comprising solution resistance (R_1/R_s), charge transfer resistance (R_{ct}), a constant phase element (CPE) representing the double-layer capacitance, and Warburg impedance (Z_w) associated with ion diffusion (see inset in Fig. 4b). Among the tested electrodes, AuSNPs/SNGCE showed the smallest semicircle in the Nyquist plot, corresponding to the lowest charge transfer resistance (R_{ct} = 221.7 Ω) compared with bare SNGCE (R_{ct} = 5004.6 Ω). This pronounced reduction in Rct reflects the enhanced electron transfer kinetics imparted by the AuSNPs. The fitted values of R_s, CPE, and Z_w for all electrode configurations are summarized in Table 1.

Collectively, these results demonstrate that the incorporation of AuSNPs significantly enhances interfacial charge transfer, reduces resistance, and improves mass transport, thereby accounting for the superior electrochemical performance observed in dopamine sensing.[56,57]

3.3 Study of the electroanalytical conditions

3.3.1 pH optimization. The pH has an impact on both the reaction and the detection of DA and 5-HT. Therefore, the influence of pH on the AuSNPs/SNGCE response towards the individual and simultaneous detection of DA and 5-HT was

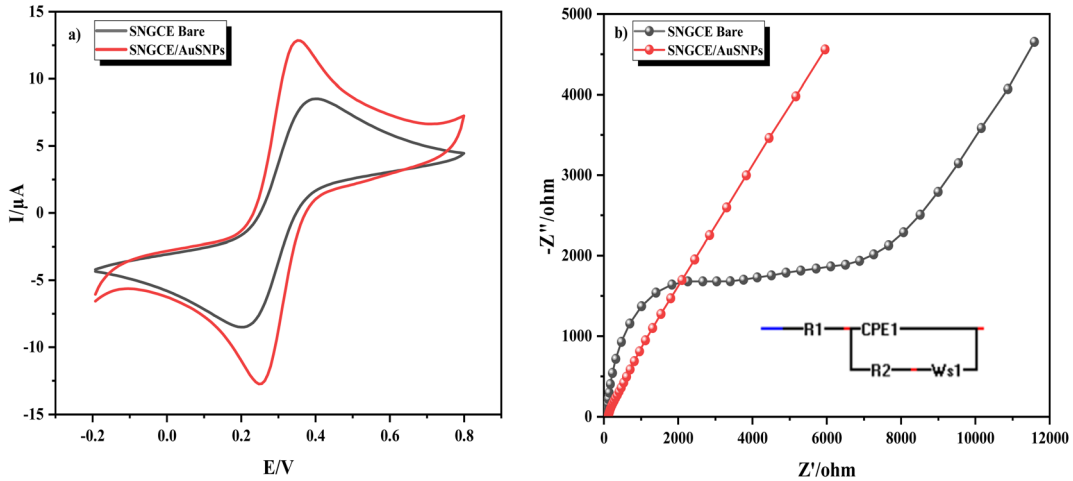

Fig. 4 (a) CVs recorded at SNGCE and SNGCE/AuSNPs in the presence of 5 mM $K_3[Fe(CN)_6]$ in 0.5 M KNO_3 aqueous solution. Potential scan rate: 0.5 V s^{-1}. (b) EIS recorded at SNGCE and SNGCE/AuNPs in the presence of 5 mM $K_3[Fe(CN)_6]/K_4[Fe(CN)_6]$ in 0.5 M KNO_3 aqueous solution. Inset: equivalent electrical circuit used in the fitting of the EIS data.

investigated using differential pulse voltammetry (DPV) within a wide range of pH (from 3 to 8). This research is essential for identifying optimal conditions for the voltammetric detection of DA and 5-HT, while also providing valuable insights into their electro–oxidation reactions by analyzing the relationship between peak potential (E_p) and pH. According to Fig. S3, the oxidation peak potentials (E_p) for both DA and 5-HT shift negatively as the pH increases from 3 to 8, due to the involvement of protons in the electrochemical process. For instance, as shown in Fig. S3a, the peak current for DA demonstrates an increase with pH until pH 8.0, after which it starts to decrease. Hence, a pH value of 8 was chosen for the rest of the study. The relationship between pH and peak potential (E_p) was found to be linear, as indicated by the equations $E_p = -0.06$ pH + 0.58 and $E_p = -0.05$ pH + 0.67 for DA and 5-HT, respectively, and with very good determination coefficients. The slopes of these equations closely approximate the theoretical value of 59 mV pH^{-1}, suggesting that the electron transfer process is coupled with an equal number of protons and electrons in the electrode reaction.

3.3.2 Individual detection

3.3.2.1 Serotonin determination. To gain a deeper understanding of the electron transfer mechanism for DA and 5-HT detection, the impact of varying scan rates on the electrochemical properties of AuSNPs/SNGCE was examined. Fig. S4a illustrates the CV voltammograms recorded at different scan rates for 5-HT in PBS (0.1 M, pH 8). Fig. S4b illustrates that the 5-HT anodic peak currents show a linear increase with the scan rate. The linear regression equation for the fitting is expressed according to the following equation: $I_p = 0.43 \times \nu + 47.59$, $R^2 = 0.98$. Similar fitting (Fig. S4c) was obtained for the anodic peak current and the square root of the studied scan rates: $I_p = 7.31 \times \nu^{\frac{1}{2}} + 22.12$, $R^2 = 0.98$. As such, confirmation was sought through plotting $\log I_p$ *versus* $\log \nu$; the resulting good fit and the slope of 0.33 (within the range 0.2–0.6) suggested that the process is controlled by the diffusion of the analyte toward the modified electrode surface.

3.3.2.2 Dopamine determination. The same experiments were conducted for the individual detection of DA. As shown in Fig. S5a, the anodic peak undergoes an increase when increasing the scan rate, which is typically the same behavior as for 5-HT molecules. From Fig. S5b and c, we observe the good linearity between the peak current and the scan rate or the square root of the scan rate; however, it was also necessary to plot $\log I_p$ *versus* $\log \nu$ (see Fig. S5d) in order to infer that the electrochemical detection of DA at the AuSNPs/SNGCE electrode is mainly governed by a diffusion-controlled process, as previously reported.

The number of electrons participating in the electrochemical reactions of these biomolecules can be assessed using the following equation:[58]

$$E = E^0 + \left(\frac{\alpha n F}{RT}\right)\log\left(\frac{RTK_0}{\alpha n F}\right) + \left(\frac{RT}{\alpha n F}\right)\log \nu \qquad (1)$$

where E^0 represents the redox potential, K_0 is the standard rate constant, n represents the number of electrons transferred, F (C mol^{-1}) stands for the Faraday constant, Q (C) denotes the

Table 1 EIS fitting parameters for SGCE and AuSNPs/SGCE using the Randles equivalent circuit

	R_s (Ω)	R_2/R_{ct} (Ω)	CPE1 (μMho)	W_{sr1} (Ω)	W_{sc1} (Ω)	n
SNGCE bare	76.429	5004.6	1.4736×10^{-6}	3439.5	2.168	0.83778
AuSNPs/SNGCE	127.55	221.7	5.6561×10^{-6}	3122.2	7.9727	0.96315

charge consumed in the electrochemical reaction, ν (V s^{-1}) represents the scan rate, and the remaining symbols retain their conventional meanings. In this case, the obtained slope was 0.38 for DA and 0.33 for 5-HT, leading to calculated αn values of 0.70 and 0.77, respectively. However, for an irreversible process, α is typically 0.5, which suggests that the number of electrons (n) involved is 2. Given that $F = 96.485$ C mol^{-1}, $R = 8.314$ J K^{-1} mol^{-1}, and $T = 298$K, the oxidation reaction mechanism of DA and 5-HT at the AuSNPs/SNGC electrodes can be inferred, as illustrated in Fig. S4e and S5e, involving the transfer of two electrons and two protons.

3.3.2.3 Individual calibration curves for both 5-HT and DA. The electrochemical behaviors of dopamine (DA) and serotonin (5-HT) were individually analyzed using the AuSNPs/SNGCE in a PBS solution (0.1 M, pH 8). Fig. 5a shows an increment in the peak current with the DA concentration.[59,60] The calibration curve for DA (inset of Fig. 5a) within the concentration range of 0.75 μM to 30 μM showed two zones of linearity: the lower concentration range (0.75 to 10 μM) modeled by the regression equation $I_p = 58.35 \times [DA] + 8.23$ ($R^2 = 0.95$), and the higher concentration range (10 to 30 μM) was modeled by the equation $I_p = 29.09 \times [DA] + 3.05$ ($R^2 = 0.99$). Similar results were found for the 5-HT analyte according to Fig. 5b and its corresponding inset. This double linear trend has also been found in other pieces of research concerning the simultaneous determination of dopamine and serotonin.[41] The concentration range tested was from 0.75 μM to 25 μM, with the following fitting for the lower concentration range: $I_p = 57.42 \times [5\text{-HT}] + 3.68$ ($R^2 = 0.99$). For the higher concentration range, $I_p = 131.11 \times [5\text{-HT}] + 2.05$ ($R^2 = 0.99$). According to these results, the sensitivities of the developed sensors are 58.35 mA M^{-1} and 131.11 mA M^{-1} for DA and 5-HT, respectively; the sensor is, therefore, about 2.5 times more sensitive to 5-HT than to DA.

3.4 The simultaneous detection of 5-HT and DA

3.4.1 Scan rate effects. The influence of the scan rate on the oxidation of DA and 5-HT was studied across a range of 10 to 70 mV s^{-1} using cyclic voltammetry in a PBS solution (0.1 M, pH 8). The cyclic voltammograms showed that the anodic current responses (I_p) increased proportionally with the scan rate (Fig. 6a). The relationships between I_p and ν for both analytes are depicted in Fig. 6b, and they can be described by the respective linear equations: I_p (5-HT) $= 1.19 \times \nu + 0.07$ ($R^2 = 0.97$) and I_p (DA) $= 1.04 \times \nu + 0.04$ ($R^2 = 0.97$). When the peak current values were plotted against the square root of the scan rates, a linear relationship was observed, with a regression coefficient of 0.99 (Fig. 6c). The results indicate that the oxidation of 5-HT and DA at the surface of the AuSNPs-modified electrode seems to be governed by diffusion, which was corroborated by the slope of the linear fitting (see Fig. 6d) between the $\log I$ *vs.* $\log \nu$ plot (between 0.4 and 0.5 for both analytes), indicating a preferably diffusion-controlled oxidation mechanism. Additionally, a positive shift in the anodic peak potential (E_p) was observed as the scan rate increased (not shown). It was found that E_p increased linearly with the natural logarithm of the scan rate. The number of electrons involved in the reaction was calculated using Laviron's equation.[36] According to this equation, the slope of the E_p *versus* $\log \nu$ plot is given by: $b = R\,T/\alpha\,n\,F$, where b is the slope and α, for a totally irreversible electrode process, is assumed to be 0.5. The calculated value for n is approximately 2, indicating that two electrons participate in the oxidation of serotonin and dopamine. Hence, the electrochemical oxidation of DA and 5-HT involves a process with two electrons and two protons.[60,61,62]

3.4.2 Calibration curves for the simultaneous detection. After conducting a detailed analysis of the individual detection of both 5-HT and DA, this section aims to provide insights into the sensor's electrochemical behavior for the simultaneous

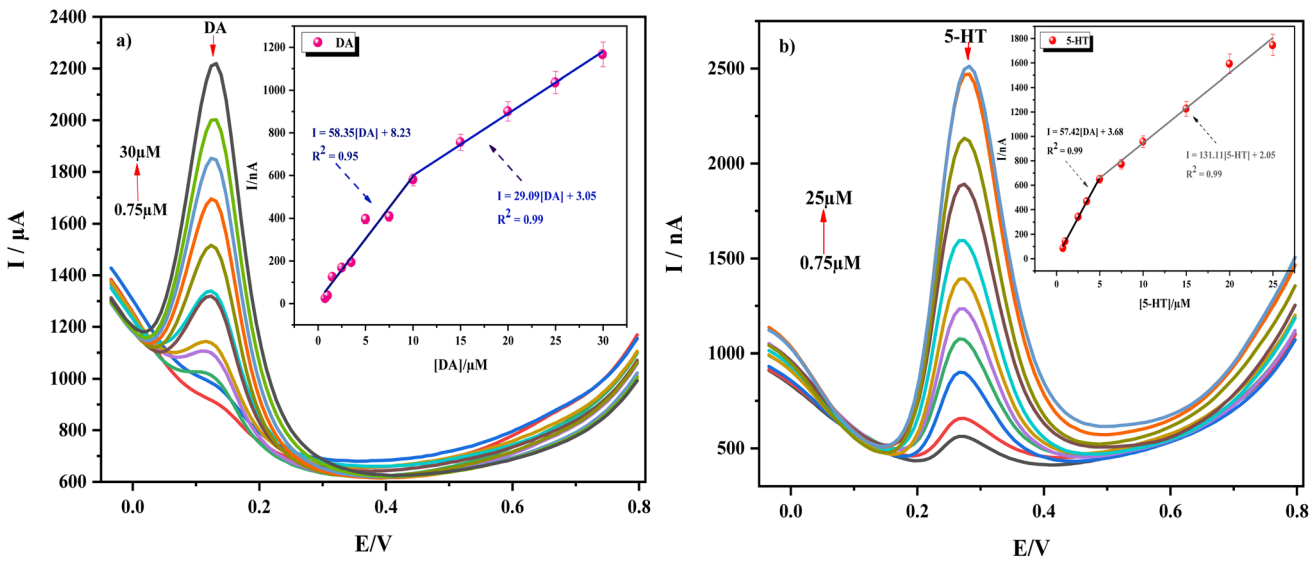

Fig. 5 (a) DPV voltammograms obtained with AuSNPs/SNGCE for the detection of (b) DA in a concentration range of (0.75–30 μM) and 5-HT in a concentration range of (0.75–25 μM), in PBS solution (0.1 M and pH 8).

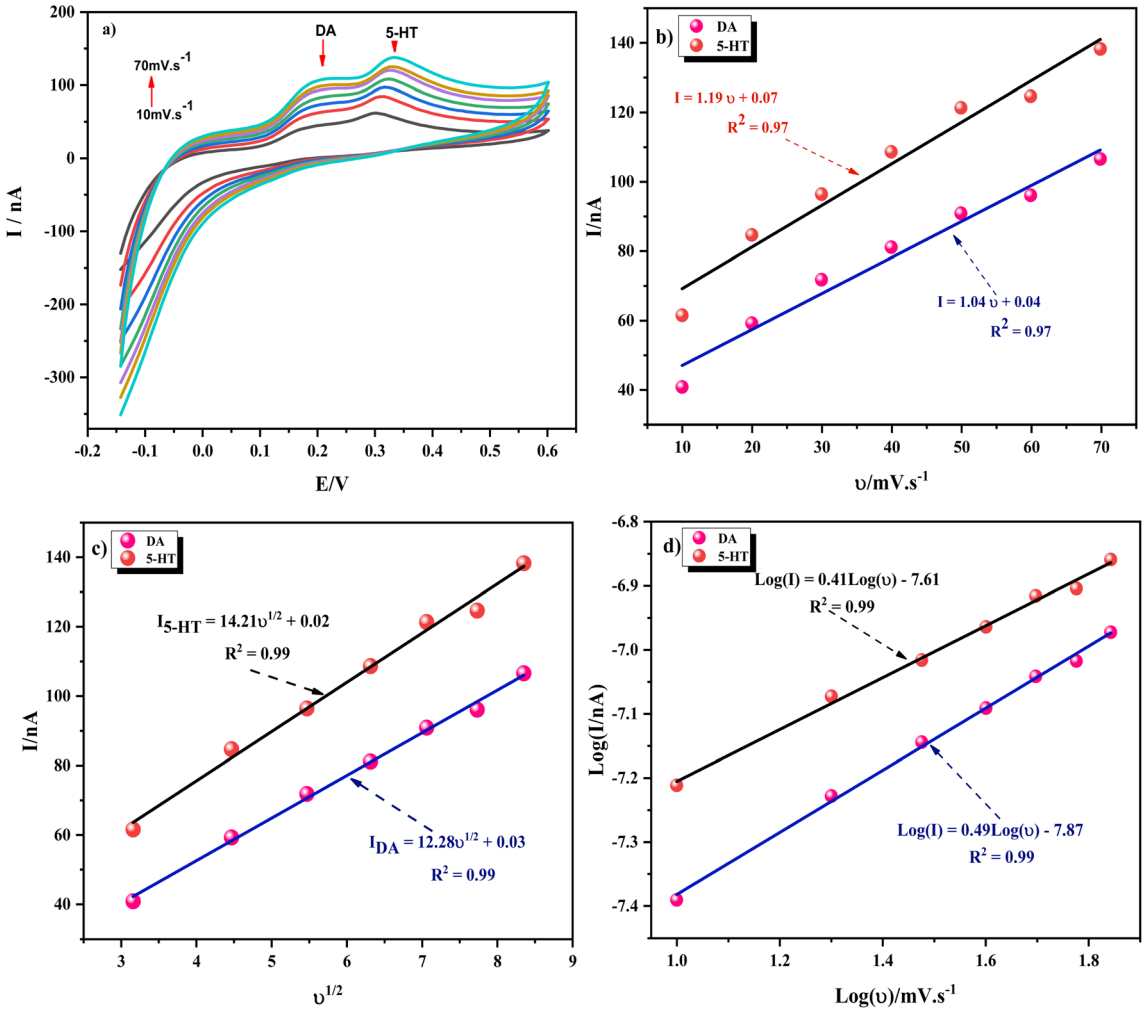

Fig. 6 (a) CV voltammograms obtained with AuSNPs/SNGCE for both 5-HT (10 μM) and DA (10 μM) in PBS (0.1 M, pH 8), at various scan rates: 10, 20, 30, 40, 50, 60 and 70 mV s^{-1}. (b) Plots of oxidation peak current, *I*, *vs.* *ν*; (c) the linear relationship between *I* and $\nu^{\frac{1}{2}}$; and (d) the linear relationship between log *I* and log *ν* for 5-HT and DA.

detection of both analytes by employing the AuSNPs/SNGCE in PBS (0.1 M, pH 8.0), at room temperature (Fig. 7). The initial tests involved determining DA and 5-HT in combined solutions, varying the concentration of one substance while keeping the other constant at the proposed electrode.

On the one hand, the calibration plot for 5-HT (see inset of Fig. 7a) resulted, as previously indicated, in two different linear zones with respect to the concentration ranges of 0.75–5 μM and 5–30 μM (with a fixed concentration of DA 0.75 μM). The respective fitting equations are as follows:

$$I_p = 210.26 \times [\text{5-HT}] - 5.79\ (R^2 = 0.98), \text{ and } I_p = 80.79 \times [\text{5-HT}] - 5.91\ (R^2 = 0.99).$$

The limit of detection (LOD) (calculated as LOD = (3 × SD_{blank})/slope, where SD_{blank} is the standard deviation of the blank) was found to be 80 pM. The limit of quantification (LOQ) (calculated as LOQ = (10 × SD_{blank})/slope, where SD_{blank} is the standard deviation of the blank) was found to be 275.37 pM. Therefore, the findings indicate that 5-HT can be detected in the presence of DA without causing any impact on the oxidation peak current and peak shape of the analyte.

On the other hand, as illustrated in Fig. 7b, the calibration plot for the determination of DA, within the linear dynamic range of 0.75–30 μM and in the presence of constant concentrations of 5-HT (0.75 μM), was obtained. Similarly, two distinct linear zones concerning the analyte concentration range were obtained: 0.75–7.5 and 7.5–30 μM. The peak current of DA exhibited a linear increase with a rise in its concentration (see the inset of Fig. 6b). The respective linear regression equations were as follows:

$$I_p = 69.01 \times [\text{DA}] + 6.09\ (R^2 = 0.92), \text{ and } I_p = 44.58 \times [\text{DA}] + 1.85\ (R^2 = 0.99),$$

with a limit of detection (LOD) of 264.7 pM and limit of quantification (LOQ) of 882.48 pM.

To evaluate the sensor effectiveness for concurrent DA and 5-HT measurements, differential pulse voltammetry (DPV) was also used to capture oxidation currents at the AuSNPs/SNGCE.

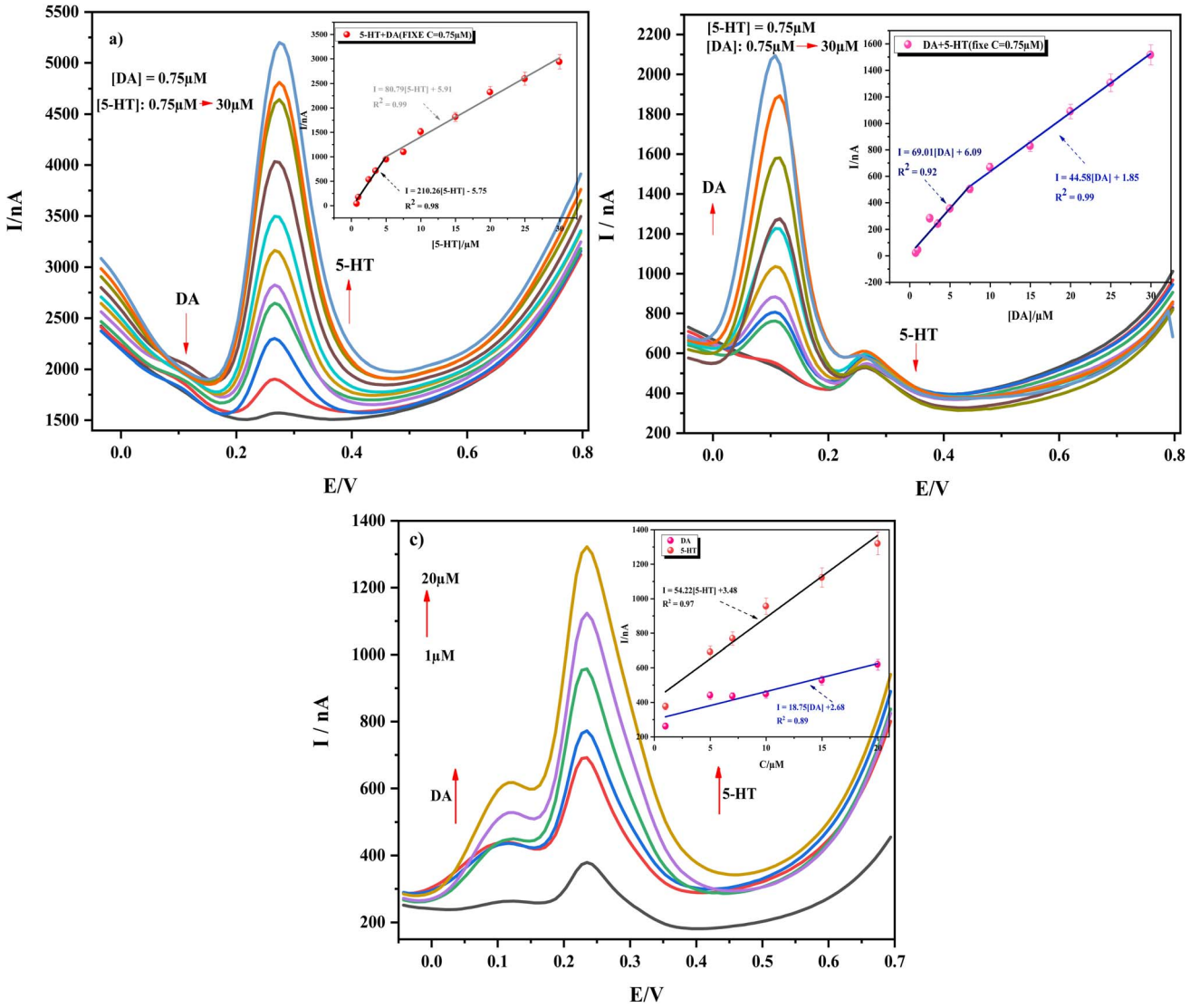

Fig. 7 (a) DPV voltammograms for different concentrations (0.75–30 μM) of 5-HT, with a fixed concentration of DA (0.75 μM). (b) DPV voltammograms of AuSNPs/SNGCE for different concentrations (0.75–30 μM) of DA, with a fixed concentration of 5-HT (0.75 μM). (c) DPV voltammograms of AuSNPs/SNGCE for the simultaneous detection of both analytes, with varying concentrations simultaneously within the common concentration range 1–20 μM. The electrode employed was AuSNPs/SNGCE in PBS solution (0.1 M and pH = 8).

According to Fig. 7c, the peak current (I_p) increases as the concentrations of both DA and 5-HT rise, while their peak potentials (E_p) remain nearly unchanged. The calibration curves for both neurotransmitters, with simultaneously varying the concentrations, exhibit linear segments within the range of 1 μM to 20 μM (see inset of Fig. 6c). The following equations can be derived for each analyte: $I_p = 54.22 \times [5\text{-HT}] + 3.48$ ($R^2 = 0.97$) and $I_p = 18.75 \times [\text{DA}] + 2.68$ ($R^2 = 0.89$). The limits of detection (LOD) were determined to be 412.80 pM and 192.55 pM ($n = 3$) for DA and 5-HT, respectively. The LOD achieved by the proposed low-cost sensor is among the lowest reported, as demonstrated by the values obtained from the literature in Table 2. Notably, our developed sensor is the only one capable of simultaneously detecting dopamine and serotonin at the nanomolar level using environmentally friendly nanoparticles as cost-effective nanomaterials.

As observed, when simultaneously detecting these two compounds, the developed sensor can achieve low detection limits and high sensitivity since target analytes like dopamine and serotonin in biological samples are typically in the nanomolar to micromolar range. The sensor LODs must be sensitive enough to detect these concentrations, highlighting the platform's detection capabilities. In general, the sensing capabilities of the suggested sensor were quite satisfactory and comparable to the performance of other electrochemical sensors utilized for detecting these two analytes according to the literature, as shown in Table 2. It is evident that the nanoplatform created in this study has an extensive linear range, closely resembling that of the majority of other sensors documented. While the limits of detection (LODs) may not be the lowest ones, they are deemed acceptable and consistent with those obtained in certain published studies, as indicated in the table. Hence, the proposed sensor is still suitable

Table 2 Electroanalytical performance of the AuSNPs/SNGCE compared to other modified electrodes reported in literature, based on different configurations[a]

Electrode materials	Electroanalytical technique	Potential/V		Linear range/μM		Limit of detection/pM		Ref.
		DA	5-HT	DA + 5-HT		DA	5-HT	
GCE/CQDs/CuO	SWV	0.05	—	10–116		15.99×10^6	—	19
CuO–Cu_2O	DPV	0.2	0.4	2–200	2–200	100×10^3	0.12×10^3	42
Co, Mo@CNFs/GCE	DPV	0.07	—	0.01–1000	—	2.35×10^3	—	62
PPyox/LSGE	DPV	0.07	—	0.05–10	—	7×10^3	—	5
AgNPs-rGO/SPCE	DPV	−0.04	0.11	10–100	10–100	7.41×10^6	7×10^6	59
$Ti_3C_2T_x$-MXene/4-APBA/SPCE	DPV	0.05	—	40–500	—	1.30×10^3	—	63
ERGO-P/GCE a	DPV	0.15	0.3	0.1–500	0.1–300	35×10^3	4.9×10^3	64
e-CS/MWCNTs/GCE	DPV	0.2	0.4	20–1000	9–1000	12×10^3	10×10^3	44
rGO-PEDOT:PSS/Nafion	DPV	0.09	0.3	0.1–50	0.1–50	0.17×10^6	0.16×10^6	40
FeC-AuNPsMWCNT/SPCE	SWV	—	0.25	0.05–20	—	17×10^3	—	65
AuSNPs/SNGCE	DPV	0.12	0.25	1–20.0	1–20.0	421.80	192.55	This work

[a] GCE/CQDs/CuO: glassy carbon electrode/carbon quantum dots/copper oxide nanocomposite. e-CS/MWCNTs: chitosan and carboxylated multi-walled carbon nanotubes. rGO-PEDOT:PSS: reduced graphene oxide, poly(3,4-ethylenedioxythiophene): polystyrene sulfonate. Co, Mo@CNFs: cobalt, molybdenum, carbon nanofibers. $Ti_3C_2T_x$-MXene/4-APBA/SPCE: titanium carbide MXene, 4-aminophenylboronic acid, screen-printed carbon electrode. ERGO-P: electrochemically reduced graphene oxide, phosphorous. FeC-AuNPsMWCNT: iron carbon, gold nanoparticles, multi-walled carbon nanotubes. AgNPs-rGO/SPCE: silver nanoparticles-decorated reduced graphene oxide, screen-printed carbon electrode. PPyox/LSGE: overoxidized polypyrrole, laser-scribed graphene electrode.

for practical applications like clinical diagnostics and therapeutic monitoring. Our approach stands out for its cost-effectiveness, eco-friendliness, high sensitivity, and electrochemical performance compared to other alternatives. The integration of bio-synthesized AuSNPs with low-cost, green transducers like Sonogel-Carbon electrodes is promising for practical applications.

3.4.3 Reproducibility, repeatability, and selectivity studies. To assess the reproducibility of the sensor fabrication, the RSD of three independently prepared AuSNPs/SNGC electrodes was calculated using DPV in a binary mixture. The RSD of anodic peak currents for 5-HT and DA was less than 4.31% and 2.21% ($n = 3$), respectively, indicating very good reproducibility (Fig. S6a). Repeatability was also evaluated by measuring the response of 5 μM DA and 5-HT with the same AuSNPs/SNGC electrode, yielding RSDs of 6.62% and 4.95% ($n = 3$), respectively, for both analytes (Fig. S6b). Furthermore, selectivity was tested by measuring 5 μM DA and 5-HT in the presence of certain interfering species (boric acid, L-tryptophan, L-tyrosine, ascorbic acid, and Ca^{2+} ions) at 100-fold higher concentrations than the neurotransmitters, as shown in Fig. S6c. These species are common in human blood (7, 58). For all of these interferents, the simultaneous detection of the dopamine and serotonin signals was only 10% different.[16] The findings demonstrated that none of the interfering species significantly affected the DA and 5-HT detection.

4 Real samples

The sensor underwent validation in preliminary clinical studies for its application in determining the concentration of neurotransmitters in real human serum across different concentration levels.

In the first step, the serum sample was diluted in PBS buffer (0.1 M, pH 7.4) at a ratio of 1 : 10. Then, the same concentrations for DA and 5-HT (3.5 μM for each) were introduced to the mixture. The initial concentrations were 2.75 μM and 12.73 μM for DA and 5-HT, respectively.

Since the concentrations of 5-HT and DA in the real serum sample were unknown, the second step involves preparing a solution with 3 μM of each analyte, dispersed in a PBS/serum mixture, to serve as the starting solution for subsequent measurements. In this case, the measured concentrations of the analytes were 5.76 μM for DA and 15.96 μM for 5-HT, respectively. The recovery was calculated using the following formula:

$$\text{Recovery}(\%) = \frac{C_{\text{analyte}+3\mu\text{M}} - C_{\text{analyte}}}{3\mu\text{M}} \quad (2)$$

and the recovery percentages and the RSD values were calculated (Table 3).

As shown in the table, the recovery percentages were very close to 100% in all the samples tested, and for both analytes,

Table 3 Recovery values of serotonin and dopamine determination in the human serum samples

Spiked sample ($n = 3$)	Added (μM)		Found (μM)		Recovery (%)		RSD	
	DA	5-HT	DA	5-HT	DA	5-HT	DA	5-HT
Sample 1	3.27	3.16	3	3	109.10%	105.40%	1.10%	1.22%
Sample 2	3.01	3.21	3	3	106.19%	107.16%	2.22%	1.96%

resulting in very low RSD values (<2%). Hence, the sensor may be promising for real sample applications in biomedical monitoring. It must be underscored that the sensor was fabricated *via* a simple drop-casting process and operates in real-time without additional conditions. Besides, it is highly cost-effective compared to similar devices, with a fabrication cost of ∼0.23 €/electrode. Its competitive pricing and strong performance make it ideal for large-scale applications.

5 Conclusions

For the first time, AuSNPs have been synthesized using pine leaf extracts and high-energy ultrasound technology, saving costs in reagents, time, and waste generated. The obtained polymorphic AuSNPs (of about 54 nm in size) were simply and easily drop-cast onto green SNGC electrodes, serving as the active layer for simultaneous DA and 5-HT detection. The electrochemical sensor demonstrated excellent electrocatalytic activity, high sensitivity, low detection limits, environmental friendliness, cost-effectiveness (∼0.23€), and fast response time. Tested at room temperature in human serum samples, the sensor's simple, green synthesis process and small nanoparticle size offer significant potential for biomedical applications, including neurotransmitter detection. These alternatives support the WHO initiatives to combat neurodegenerative diseases like Alzheimer's and cancer through research, prevention, diagnosis, and treatment.

Author contributions

Asma Blel: conceptualization, methodology investigation, visualization, formal analysis, writing – original draft. Juan José García-Guzmán: conceptualization, methodology, validation, formal analysis, writing – review & editing, supervision, funding acquisition. Laura Cubillana-Aguilera: conceptualization, methodology, validation, formal analysis, writing – review & editing, supervision, funding acquisition. José María Palacios-Santander: conceptualization, methodology, validation, formal analysis, writing – review & editing, supervision, funding acquisition, project administration Chérif Dridi: conceptualization, methodology, validation, formal analysis, supervision, funding acquisition, project administration.

Conflicts of interest

The authors declare that they have no known competing financial interests or personal relationships that could have appeared to influence the work reported in this paper.

Ethical approval

All the studies involving research work applied to biological samples (human blood, plasma, and/or serum) were conducted in accordance with the Declaration of Helsinki and the "Multibioanalysis" research project (Proyecto de Generación del Conocimiento, PID2021-122578NB-I00) financed by MCIN/AEI/10.13039/501100011033/FEDER, EU "ERDF: A way of making Europe". Consequently, the present study, in accordance with the Spanish regulation 'Real Decreto 1090/2015, de 4 de diciembre, por el se regulan los ensayos clínicos con medicamentos, los Comités de Ética de la Investigación con medicamentos y el Registro Español de Estudios Clínicos', was approved by the Research Ethics Committee of Cadiz (Spain), on May 12, 2023, registry/protocol number 15.23. In this approval, the resolution stated that the aforementioned projects involving human samples are viable, demonstrate sufficient methodological rigor, present appropriate evaluation of economic costs, and, with respect to the ethical aspects, meet the necessary requirements of suitability of the protocol in relation to the objectives of the study, including obtaining informed consent of all the donors prior to the procedures.

Data availability

Data will be made available upon reasonable request.

Supplementary information: additional figures and plots. Fig. S1 is real image of solutions before and after AuSNPs formation. The change in color from yellowish to red supports the evidence of AuSNPs formation. The AuSNPs presence is further validated through SEM images in Fig. S2, in which a back-scattered electron detector was employed with an emission gun at 10 kV. As an initial step in the analysis, Fig. S3 presents the pH optimisation of DA and 5-HT separately. This optimization is essential to identify the pH conditions that maximize the redox response and ensure clear peak separation between the two analytes. In the continuation, Fig. S4 and S5 present the scan rate responses corresponding to the individual detection of 5-HT and DA respectively. This analysis is essential to optimize the electrochemical conditions and to understand how each analyte responds independently before studying their simultaneous detection. Fig. S6 presents the evaluation of the analytical performance of the AuSNPs/SNGCE electrode in PBS solution (0.1 M, pH toward the simultaneous detection of 5 μM DA and 5-HT. As shown, panel (a) investigates reproducibility using three independently fabricated sensors, panel (b) examines repeatability through three successive measurements with the same sensor, and panel (c) assesses selectivity in the presence of potential interferents such as boric acid (BA), L-tryptophan (L-trp), L-tyrosine (L-tyr), calcium ions (Ca^{2+}), and ascorbic acid (AA) at 100-fold higher concentrations. These assessments demonstrate the robustness and reliability of the sensor, confirming its potential for accurate detection of DA and 5-HT in complex biological environments. Finally, Fig. S7 shows the optimization of DPV parameters, including interval time, modulation amplitude, and step potential, for the detection of DA and 5-HT. Adjusting these parameters was necessary to maximize peak current intensity and resolution, ensuring accurate and sensitive determination of both analytes. See DOI: **https://doi.org/10.1039/d5ra04658k**.

Acknowledgements

The authors thank the FQM-169 research group for the support given regarding the ATR-FTIR spectra acquisition. The authors also acknowledge the Electron Microscopy Division of the

Servicios Centrales de Investigación Científica y Tecnológica at the University of Cadiz (SCICYT-UCA) for their technical assistance during SEM measurements. Additionally, the authors acknowledge Dr Zied Bouraoui for performing the human blood preparation procedures. Tunisian authors would like to thank the Tunisian MHESR for supporting part of this work and the University of Sousse for the "Bourse d'alternance" fellowship awarded to Ms. Asma Blel. Spanish authors thank the Agencia Estatal de Investigación (AEI), the Ministerio de Ciencia e Innovación of Spain, and FEDER funds (EU) for the "Multibioanalysis" research project (Proyecto de Generación del Conocimiento, PID2021-122578NB-I00) financed by MCIN/AEI/10.13039/501100011033/FEDER, EU "ERDF: A way of making Europe". They also thank "Plan Propio 2022–2023" from the University of Cadiz for providing funding through the "Acceso al uso de Servicios Centrales de Investigación. Financiación de Actividades" (Ref: SC2023-001) and the "Proyectos Noveles para Impulsar su Carrera Científica" (Ref: PR2022-025, SENSPOT and PR2023-07, 3DLACBIOSENS) programs. Finally, funds provided by Junta de Andalucía through the University of Cadiz (Research Groups Call 'PAIDI, 2022 and 2023') are acknowledged.

References

1 M. Hasanzadeh, N. Shadjou and E. Omidinia, A novel electroanalytical method for simultaneous detection of two neurotransmitter dopamine and serotonin in human serum, *J. Neurosci. Methods*, 2013, **219**(1), 52–60, DOI: 10.1016/j.jneumeth.2013.07.007.

2 E. Rand, et al., A carbon nanofiber based biosensor for simultaneous detection of dopamine and serotonin in the presence of ascorbic acid, *Biosens. Bioelectron.*, 2013, **42**(1), 434–438, DOI: 10.1016/j.bios.2012.10.080.

3 Z. Hui, W. Lai-Fa, W. Xue-Qin, D. Ling, H. Bin-Sheng and J.-M. Li, Mechanisms and therapeutic potential of chinonin in nervous system diseases, *J. Asian Nat. Prod. Res.*, 2024, **26**(12), 1405–1420, DOI: 10.1080/10286020.2024.2371040.

4 S. A. Leau, C. Lete, C. Matei and S. Lupu, Electrochemical Sensing Platform Based on Metal Nanoparticles for Epinephrine and Serotonin, *Biosensors*, 2023, **13**(8), 781, DOI: 10.3390/bios13080781.

5 A. Berni, A. Ait Lahcen, K. N. Salama and A. Amine, 3D-porous laser-scribed graphene decorated with overoxidized polypyrrole as an electrochemical sensing platform for dopamine, *J. Electroanal. Chem.*, 2022, **919**, 116529, DOI: 10.1016/j.jelechem.2022.116529.

6 N. Mahdi, M. Roushani and Z. M. Karazan, Electrochemical sensor based on molecularly imprinted copolymer for selective and simultaneous determination of riboflavin, dopamine, and L-tryptophan, *J. Mol. Recognit.*, 2023, **36**(10), e3053, DOI: 10.1002/jmr.3053.

7 C. Sarkar, D. Chakroborty, U. R. Chowdhury, P. S. Dasgupta and S. Basu, Dopamine increases the efficacy of anticancer drugs in breast and colon cancer preclinical models, *Clin. Cancer Res.*, 2008, **14**(8), 2502–2510, DOI: 10.1158/1078-0432.CCR-07-1778.

8 K. K. de L. Augusto, et al., Electrochemical sensor based on carbon nanohorns and hydrophobic deep eutectic solvent for the determination of serotonin in biological samples, *Electrochim. Acta*, 2025, **520**, 145836, DOI: 10.1016/j.electacta.2025.145836.

9 M. Mehdi Foroughi, S. Jahani and S. Rashidi, Simultaneous detection of ascorbic acid, dopamine, acetaminophen and tryptophan using a screen-printed electrode modified with woolen ball-shaped La^{3+}/TiO_2 nanostructure as a quadruplet nanosensor, *Microchem. J.*, 2024, **198**, 110156, DOI: 10.1016/j.microc.2024.110156.

10 J. Ferreira, R. Peres, M. Nakamura, H. Toma and T. Canevari, PdNPs/carbon dots/silica hybrid nanostructures: the development of an electrochemical sensor for simultaneous determination of dopamine and serotonin in real samples, *J. Nanopart. Res.*, 2023, **25**(9), DOI: 10.1007/s11051-022-05659-1.

11 Z. Aryan, H. Khajehsharifi and S. Shahrokhian, AuNPs-Ultrathin/Graphitic-C3N4 nanosheets as a sensitive platform for electrochemical detection and determination of dopamine, *Microchem. J.*, 2024, **198**, 110087, DOI: 10.1016/j.microc.2024.110087.

12 P. Balakrishna, S. George, H. Hatoum and S. Mukherjee, Serotonin pathway in cancer, *Int. J. Mol. Sci.*, 2021, **22**(3), 1–10, DOI: 10.3390/ijms22031268.

13 M. Moslah, Z. Fredj and C. Dridi, Development of a new highly sensitive serotonin sensor based on green synthesized silver nanoparticle decorated reduced graphene oxide, *Anal. Methods*, 2021, **13**(43), 5187–5194, DOI: 10.1039/d1ay01532j.

14 D. Nowicka, M. Kubicki, V. Patroniak, T. Łuczak and A. Gorczyński, Self-assembly of simple Schiff base ligand into unique saddle-type [4x4] tetranuclear architecture and its application as selective voltammetric dopamine sensor in aqueous conditions, *Electrochim. Acta*, 2024, **476**, 1–12, DOI: 10.1016/j.electacta.2023.143754.

15 X. Cheng, et al., Metabolomics of Non-muscle Invasive Bladder Cancer: Biomarkers for early detection of bladder cancer, *Front. Oncol.*, 2018, **8**, 1–11, DOI: 10.3389/fonc.2018.00494.

16 M. Talbi, A. Anurag, C. Tegenkamp, M. Ben Ali and O. Kanoun, Enhanced electrochemical detection of nitrite and nitrate in water using Chitosan-Copper phthalocyanine nanocomposite, *Measurement*, 2024, **238**, 115395, DOI: 10.1016/j.measurement.2024.115395.

17 D. Chakroborty, C. Sarkar, R. B. Mitra, S. Banerjee, P. S. Dasgupta and S. Basu, Depleted dopamine in gastric cancer tissues: Dopamine treatment retards growth of gastric cancer by inhibiting angiogenesis, *Clin. Cancer Res.*, 2004, **10**(13), 4349–4356, DOI: 10.1158/1078-0432.CCR-04-0059.

18 P. Dowling, et al., Elevated levels of 14-3-3 proteins, serotonin, gamma enolase and pyruvate kinase identified in clinical samples from patients diagnosed with colorectal cancer, *Clin. Chim. Acta*, 2015, **441**, 133–141, DOI: 10.1016/j.cca.2014.12.005.

19 S. E. Elugoke, O. E. Fayemi, A. S. Adekunle, P. S. Ganesh, S. Y. Kim and E. E. Ebenso, Sensitive and selective neurotransmitter epinephrine detection at a carbon quantum dots/copper oxide nanocomposite, *J. Electroanal. Chem.*, 2023, **929**, 117120, DOI: 10.1016/j.jelechem.2022.117120.

20 V. Kannen, M. Bader, J. Y. Sakita, S. A. Uyemura and J. A. Squire, The Dual Role of Serotonin in Colorectal Cancer, *Trends Endocrinol. Metab.*, 2020, **31**(8), 611–625, DOI: 10.1016/j.tem.2020.04.008.

21 A. Yılmaz Kabaca, M. Bilgi Kamaç, M. Yılmaz and T. Atıcı, Ultra-sensitive electrochemical sensors for simultaneous determination of dopamine and serotonin based on titanium oxide-gold nanoparticles-poly Nile blue (in deep eutectic solvent), *Electrochim. Acta*, 2023, **467**, 143046, DOI: 10.1016/j.electacta.2023.143046.

22 A. M. Fekry, S. M. Azab, F. M. Abou Attia, N. S. Ibrahim and G. G. Mohamed, An innovative sensor for the electrochemical determination of the new melatonergic antidepressant drug agomelatine, *Measurement*, 2021, **186**, 110160, DOI: 10.1016/j.measurement.2021.110160.

23 Y. Gao, Y. Wang, J. Jiang, P. Wei and H. Sun, Triggered 'On/off' Luminescent Polypeptide Bowl-Shaped Nanoparticles for Selective Lighting of Tumor Cells, *Small*, 2025, **21**(11), 2411432, DOI: 10.1002/smll.202411432.

24 C. Gao, H. Sun and J. Du, Unusual Endotaxy Growth of Hexagonal Nanosheets by the Self-Assembly of a Homopolymer, *Angew. Chem., Int. Ed.*, 2025, **64**(7), e202420079, DOI: 10.1002/anie.202420079.

25 N. Zhang, et al., Association between serum vitamin D level and cardiovascular disease in Chinese patients with type 2 diabetes mellitus: a cross-sectional study, *Sci. Rep.*, 2025, **15**(1), 6454, DOI: 10.1038/s41598-025-90785-8.

26 N. Ben Messaoud, M. E. Ghica, C. Dridi, M. Ben Ali and C. M. A. Brett, Electrochemical sensor based on multiwalled carbon nanotube and gold nanoparticle modified electrode for the sensitive detection of bisphenol A, *Sens. Actuators, B*, 2017, **253**, 513–522, DOI: 10.1016/j.snb.2017.06.160.

27 S. Jebril, M. de V. García-Moreno, J. M. Palacios-Santander, C. Dridi and L. Cubillana-Aguilera, Development of a cost-effective and sustainable nanoplatform based on a green gold sononanoparticles/carbon black nanocomposite for high-performance simultaneous determination of nanoplastics, *Environ. Sci.: Nano*, 2022, **9**(8), 3126–3138, DOI: 10.1039/d2en00424k.

28 M. R. de Barros, J. P. Winiarski, W. C. Elias, C. E. M. de Campos and C. L. Jost, Au-on-Pd bimetallic nanoparticles applied to the voltammetric determination and monitoring of 4-nitroaniline in environmental samples, *J. Environ. Chem. Eng.*, 2021, **9**(5), 105821, DOI: 10.1016/j.jece.2021.105821.

29 A. Blel, M. Echabaane and C. Dridi, Development of an electrochemical nanoplatform based on ZnO nanoparticles and carbon black nanocomposite for the detection of tryptophan, *J. Solid State Electrochem.*, 2024, **28**(8), 2727–2740, DOI: 10.1007/s10008-024-05830-9.

30 J. Qiao and L. Qi, Recent progress in plant-gold nanoparticles fabrication methods and bio-applications, *Talanta*, 2021, **223**(45), 121396, DOI: 10.1016/j.talanta.2020.121396.

31 F. E. Ettadili, et al., Recent advances in the nanoparticles synthesis using plant extract: Applications and future recommendations, *J. Mol. Struct.*, 2022, **1248**, 131538, DOI: 10.1016/j.molstruc.2021.131538.

32 E. G. Döll, E. R. Santana, J. P. Winiarski, L. G. Baumgarten and I. C. Vieira, Green Synthesis of Gold Nanoparticles Using Peach Extract Incorporated in Graphene for the Electrochemical Determination of Antioxidant Butylated Hydroxyanisole in Food Matrices, *Biosensors*, 2023, **13**(12), 1037, DOI: 10.3390/bios13121037.

33 G. A. Vinnacombe-Willson, Y. Conti, A. Stefancu, P. S. Weiss, E. Cortés and L. Scarabelli, Direct Bottom-Up *In Situ* Growth: A Paradigm Shift for Studies in Wet-Chemical Synthesis of Gold Nanoparticles, *Chem. Rev.*, 2023, **123**(13), 8488–8529, DOI: 10.1021/acs.chemrev.2c00914.

34 C. Daruich De Souza, B. Ribeiro Nogueira and M. E. C. M. Rostelato, Review of the methodologies used in the synthesis gold nanoparticles by chemical reduction, *J. Alloys Compd.*, 2019, **798**, 714–740, DOI: 10.1016/j.jallcom.2019.05.153.

35 K. Krishnaswamy and V. Orsat, Insight into the nanodielectric properties of gold nanoparticles synthesized from maple leaf and pine needle extracts, *Ind. Crops Prod.*, 2015, **66**, 131–136, DOI: 10.1016/j.indcrop.2014.12.048.

36 S. Rantataro, I. Parkkinen, M. Airavaara and T. Laurila, Real-time selective detection of dopamine and serotonin at nanomolar concentration from complex *in vitro* systems, *Biosens. Bioelectron.*, 2023, **241**, 115579, DOI: 10.1016/j.bios.2023.115579.

37 S. Jebril, L. Cubillana-Aguilera, J. M. Palacios-Santander and C. Dridi, A novel electrochemical sensor modified with green gold sononanoparticles and carbon black nanocomposite for bisphenol A detection, *Mater. Sci. Eng., B*, 2021, **264**(62), 114951, DOI: 10.1016/j.mseb.2020.114951.

38 R. Geetha, T. Ashokkumar, S. Tamilselvan, K. Govindaraju, M. Sadiq and G. Singaravelu, Green synthesis of gold nanoparticles and their anticancer activity, *Cancer Nanotechnol.*, 2013, **4**(4–5), 91–98, DOI: 10.1007/s12645-013-0040-9.

39 J. Suriyaprakash, et al., Precise surface molecular engineering of 2D-Bi2S3 enables the ultrasensitive simultaneous detection of dopamine, epinephrine, serotonin and uric acid, *Surf. Interfaces*, 2024, **46**, 104021, DOI: 10.1016/j.surfin.2024.104021.

40 S. H. Ko, S. W. Kim, S. H. Lee and Y. J. Lee, Electrodeposited reduced graphene oxide-PEDOT:PSS/Nafion hybrid interface for the simultaneous determination of dopamine and serotonin, *Sci. Rep.*, 2023, **13**(1), 1–11, DOI: 10.1038/s41598-023-47693-6.

41 F. Fazl and M. B. Gholivand, High performance electrochemical method for simultaneous determination dopamine, serotonin, and tryptophan by ZrO2–CuO co-

doped CeO2 modified carbon paste electrode, *Talanta*, 2022, **239**, 122982, DOI: 10.1016/j.talanta.2021.122982.

42 A. Salova, S. F. Mahmud, N. K. A. Almasoudie, N. Mohammed, A. A. Albeer and R. F. Amer, CuO-Cu2O nanostructures as a sensitive sensing platform for electrochemical sensing of dopamine, serotonin, acetaminophen, and caffeine substances, *Inorg. Chem. Commun.*, 2024, **161**, 112065, DOI: 10.1016/j.inoche.2024.112065.

43 S. Tang, M. Liu, W. Wang, A. Liang, F. Zhang and A. Luo, An amorphous zinc/copper double transition metal hydroxides for electrochemical simultaneous detection of dopamine, serotonin, and melatonin, *New J. Chem.*, 2023, **47**(35), 16337–16344, DOI: 10.1039/d3nj02297h.

44 S. Tang, A. Liang, M. Liu, W. Wang, F. Zhang and A. Luo, A glassy carbon electrode modified with a composite consisting of electrodeposited chitosan and carboxylated multi-walled carbon nanotubes for simultaneous voltammetric determination of dopamine, serotonin and melatonin, *Carbon Lett.*, 2023, **33**(7), 2129–2139, DOI: 10.1007/s42823-023-00556-6.

45 G. Singh, A. Kushwaha and M. Sharma, Highly sensitive and selective detection of serotonin and dopamine with stable oxidation potentials using novel Dy2MoO6 nanosheets, *Mater. Chem. Phys.*, 2022, **279**, 125782, DOI: 10.1016/j.matchemphys.2022.125782.

46 M. A. Fathy and P. Bühlmann, Next-Generation Potentiometric Sensors: A Review of Flexible and Wearable Technologies, *Biosensors*, 2025, **15**(1), 51, DOI: 10.3390/bios15010051.

47 L. M. Cubillana-Aguilera, J. M. Palacios-Santander, I. Naranjo-Rodríguez and J. L. Hidalgo-Hidalgo-De-Cisneros, Study of the influence of the graphite powder particle size on the structure of the Sonogel-carbon materials, *J. Sol-Gel Sci. Technol.*, 2006, **40**(1), 55–64, DOI: 10.1007/s10971-006-9151-7.

48 H. Aldewachi, T. Chalati, M. N. Woodroofe, N. Bricklebank, B. Sharrack and P. Gardiner, Gold nanoparticle-based colorimetric biosensors, *Nanoscale*, 2018, **10**(1), 18–33, DOI: 10.1039/c7nr06367a.

49 E. Ferrari, Gold Nanoparticle-Based Plasmonic Biosensors, *Biosensors*, 2023, **13**, 411, DOI: 10.3390/bios13030411.

50 S. Bhattacharjee, DLS and zeta potential – What they are and what they are not?, *J. Controlled Release*, 2016, **235**, 337–351, DOI: 10.1016/j.jconrel.2016.06.017.

51 F. S. Sharopov, H. Zhang and W. N. Setzer, Composition of geranium (*Pelargonium graveolens*) essential oil from Tajikistan, *Am. J. Essent. Oil. Nat. Prod.*, 2014, **2**(22), 13–16.

52 N. Thangamani and N. Bhuvaneshwari, Green synthesis of gold nanoparticles using Simarouba glauca leaf extract and their biological activity of micro-organism, *Chem. Phys. Lett.*, 2019, **732**, 136587, DOI: 10.1016/j.cplett.2019.07.015.

53 S. Rashid, M. Azeem, S. A. Khan, M. M. Shah and R. Ahmad, Characterization and synergistic antibacterial potential of green synthesized silver nanoparticles using aqueous root extracts of important medicinal plants of Pakistan, *Colloids Surf., B*, 2019, **179**, 317–325, DOI: 10.1016/j.colsurfb.2019.04.016.

54 C. Bartolucci, et al., Green nanomaterials fostering agrifood sustainability, *TrAC, Trends Anal. Chem.*, 2020, **125**, 115840, DOI: 10.1016/j.trac.2020.115840.

55 F. Khan, M. Shariq, M. Asif, M. A. Siddiqui, P. Malan and F. Ahmad, Green Nanotechnology: Plant-Mediated Nanoparticle Synthesis and Application, *Nanomaterials*, 2022, **12**(4), 673, DOI: 10.3390/nano12040673.

56 A. Karnwal, et al., Gold Nanoparticles in Nanobiotechnology: From Synthesis to Biosensing Applications, *ACS Omega*, 2024, **9**(28), 29966–29982, DOI: 10.1021/acsomega.3c10352.

57 G. Selvolini, C. Lazzarini and G. Marrazza, Electrochemical Nanocomposite Single-Use Sensor for Dopamine Detection, *Sensors*, 2019, **19**(14), 3097, DOI: 10.3390/s19143097.

58 C. Zeng, et al., Simultaneous detection of norepinephrine and 5-hydroxytryptophan using poly-alizarin/multi-walled carbon nanotubes-graphene modified carbon fiber microelectrode array sensor, *Talanta*, 2024, **270**, 125565, DOI: 10.1016/j.talanta.2023.125565.

59 M. Moslah and C. Dridi, Development of An Eco-Friendly and Cost-Effective Electrochemical Sensor for the Simultaneous Detection of Dopamine and Serotonin, *J. Electrochem. Soc.*, 2024, **171**(6), 067506, DOI: 10.1149/1945-7111/ad537f.

60 S. N. Cuhadar, H. Durmaz and N. Yildirim-Tirgil, Multi-detection of seratonin and dopamine based on an electrochemical aptasensor, *Chem. Pap.*, 2024, **78**(12), 7175–7185, DOI: 10.1007/s11696-024-03598-w.

61 A. Babaei and A. R. Taheri, Nafion/Ni(OH)$_2$ nanoparticles-carbon nanotube composite modified glassy carbon electrode as a sensor for simultaneous determination of dopamine and serotonin in the presence of ascorbic acid, *Sens. Actuators, B*, 2013, **176**, 543–551, DOI: 10.1016/j.snb.2012.09.021.

62 Y. Xing, et al., Sensitive sensing platform based on Co, Mo doped electrospun nanofibers for simultaneous electrochemical detection of dopamine and uric acid, *Talanta*, 2024, **271**, 125674, DOI: 10.1016/j.talanta.2024.125674.

63 S. G. Chavan, P. R. Rathod, A. Koyappayil, A. Go and M. H. Lee, Two-step' signal amplification for ultrasensitive detection of dopamine in human serum sample using Ti3C2Tx-MXene, *Sens. Actuators, B*, 2024, **404**(77), 135308, DOI: 10.1016/j.snb.2024.135308.

64 H. S. Han, H. K. Lee, J. M. You, H. Jeong and S. Jeon, Electrochemical biosensor for simultaneous determination of dopamine and serotonin based on electrochemically reduced GO-porphyrin, *Sens. Actuators, B*, 2014, **190**, 886–895, DOI: 10.1016/j.snb.2013.09.022.

65 S. Kumar, A. K. Bhagat, M. Bhaiyya, K. Amreen, S. K. Dubey and S. Goel, A Machine Learning Approach for Simultaneous Electrochemical Detection of Dopamine and Serotonin in an Optimized Carbon Thread-Based Miniaturized Device, *IEEE Sens. J.*, 2024, **24**(13), 21378–21385, DOI: 10.1109/JSEN.2024.3386655.